

Valence holes as Luttinger spinor based qubits in quantum dots

Chang-Yu Hsieh,^{1,2} Ross Cheriton,^{1,2} Marek Korkusinski,¹ and Pawel Hawrylak^{1,2}

¹*Quantum Theory Group, Institute for Microstructural Sciences,
National Research Council, Ottawa, ON, Canada K1A 0R6*

²*Department of Physics, University of Ottawa, Ottawa, ON, Canada, K1N 6N5*

Abstract

We present a theory of valence holes as Luttinger spinor based qubits in p-doped self-assembled quantum dots within the 4-band $k \cdot p$ formalism. The two qubit levels are identified with the two chiralities of the doubly degenerate ground state. We show that single qubit operations can be implemented with static magnetic field applied along the z axis (growth direction) for $\hat{\sigma}_z$ operation and with magnetic field in the quantum dot plane, x direction, for $\hat{\sigma}_x$ operation. The coupling of two dots and hence the double qubit operations are shown to be sensitive to the orientation of the two quantum dots. For vertical qubit arrays, there exists an optimal qubit separation suitable for the voltage control of qubit-qubit interactions.

I. INTRODUCTION

There is currently interest in using single electron spins in quantum dots (QDs) for quantum information processing (QIP) applications¹⁻⁶. In *III-V* semiconductor quantum dots, such as *GaAs*, spins of conduction band electrons couple to nuclear spins of the host material and suffer decoherence due to hyperfine interactions. However, valence hole states are built from atomic *p*-type orbitals, which are expected to minimize the hyperfine interaction between the hole and surrounding nuclear spins⁷. The spin of a valence hole as a qubit is expected to have longer coherence time. A theory of heavy holes as qubits has been developed in the single band approximation⁷⁻⁹. The justification for the use of the heavy hole single band approximation is that strain and QD confinement suppress the coupling between heavy hole (HH) and light hole (LH) bands. Under such an assumption, the qubit levels are defined by the $J_z = +3/2$ and $J_z = -3/2$ HH states.

In such a simple model, the exchange coupling J needed to generate entanglement between spins of two holes is proportional to t^2/U , where t is the tunneling strength of the hole and U is the on-site Coulomb energy. However, recent theoretical¹⁰ and experimental¹¹ work show that in two vertically coupled disk-like QDs the spin orbit (SO) coupling between HH and LH bands changes the sign of the effective tunneling matrix element t as a function of inter-dot distance. If the inter-dot distance is smaller than a critical value, the hole state is mainly symmetric. However, if the inter-dot distance passes the critical value, the hole state is mainly antisymmetric. These results suggest that a description of an array of hole-based qubits requires taking into account the hole tunneling between dots with SO coupling between HH and LH bands. The theory of valence holes in quantum dots with strong SO coupling has been developed already¹²⁻¹⁷. In this theory hole spin is strongly coupled to orbital motion and valence hole states are treated as Luttinger spinors. The two HH ground states are replaced by two Luttinger spinors¹² with different chiralities.

In this work, we develop a theory of qubits based on the chirality of the valence hole-based Luttinger spinors. We are particularly interested in square-like self-assembled quantum dots grown on nanotemplates¹⁸, which due to scalable architecture may lead to quantum information processing devices. We start with a single hole confined in an isolated QD. We explicitly define the qubit as two chirality states of Luttinger spinor and show how to perform single qubit operations. Our theory reproduces results obtained earlier by Kyrychenko and

Kossut¹³. Next, we investigate the tunneling of a valence hole in two orientations of two coupled square QDs as illustrated in Fig 1. The tunneling barriers for vertically coupled quantum dots (VCQDs) and laterally coupled quantum dots (LCQDs) are modelled as finite potential wells, as shown in Fig 1. The tunnel barrier strength is characterized by the band-offset between the dot and the barrier material. For VCQDs, we verify the results¹¹ obtained for disk quantum dots showing the reversal of ground state character from symmetric to antisymmetric as a function of inter-dot distance. Close to the reversal, the vanishing of tunneling of a Luttinger spinor hole in VCQDs allows the benefit of strong confinement defined by growth with the possibility to control tunneling and hence double qubit operations using additional metallic gates.

II. MODEL

Following Ref. 12, we expand the wavefunction of a valence hole confined to a nanostructure defined by confining potential $V(\mathbf{r})$ in terms of $J_z = 3/2, -1/2, 1/2, -3/2$ Bloch basis functions. The 4-band Luttinger Kohn (LK) Hamiltonian¹⁹ reads,

$$\hat{H}_{LK} = \begin{pmatrix} \hat{P}^+ & \hat{R} & -\hat{S} & 0 \\ \hat{R}^* & \hat{P}^- & 0 & \hat{S} \\ -\hat{S}^* & 0 & \hat{P}^- & \hat{R} \\ 0 & \hat{S}^* & \hat{R}^* & \hat{P}^+ \end{pmatrix} + V(\mathbf{r})\mathbf{I} + \kappa\Omega\mathbf{J} \cdot \hat{\mathbf{B}}, \quad (1)$$

where \mathbf{I} is the identity matrix, \hbar is Planck's constant, $\Omega = \hbar eB/m_0c$ is the cyclotron energy, and κ is a material parameter. $V(\mathbf{r})$ represents a 3D infinite potential well in case of a single QD in this study. The operator \mathbf{J} is the angular momentum operator for spin 3/2 particle defined in Ref. 19. The operators in Eq.(1) are defined as follows

$$\begin{aligned} \hat{P}^+ &= \frac{\hbar^2}{2m_0}[(\gamma_1 + \gamma_2)(\Pi_x^2 + \Pi_y^2) + (\gamma_1 - 2\gamma_2)\Pi_z^2], \\ \hat{P}^- &= \frac{\hbar^2}{2m_0}[(\gamma_1 - \gamma_2)(\Pi_x^2 + \Pi_y^2) + (\gamma_1 + 2\gamma_2)\Pi_z^2], \\ \hat{R} &= \frac{\hbar^2}{2m_0}(-\sqrt{3})\gamma_{23}\Pi_-^2, \\ \hat{S} &= \frac{\hbar^2}{2m_0}(2\sqrt{3})\gamma_3\Pi_- \Pi_z, \end{aligned} \quad (2)$$

where $\gamma_{1,2,3}$ represent the Luttinger material parameters, $\gamma_{23} = (\gamma_2 + \gamma_3)/2$, $\Pi_a = k_a - (e/c\hbar)(\mathbf{A})_a$, $k_a = -i\frac{\partial}{\partial a}$, $a = x, y, z$, and $k_- = k_x - ik_y$. For this study, we choose In-

GaAs/GaAs QDs. The InGaAs Luttinger material parameters are $\gamma_1 = 11.01$, $\gamma_2 = 4.18$, and $\gamma_3 = 4.84$. The subscript 0 means no external field in this study.

The LK Hamiltonian in Eq.(1) exhibits several symmetries that we use to characterize the Luttinger spinors (the eigenstates of the LK Hamiltonian). The confining potential along the z direction is symmetric with respect to the origin defined in the middle of the structure; yet, due to spin-orbit coupling between different bands, our system does not have definite parity symmetry along the z direction but the time reversal symmetry of the system demands the two HH bands have opposite parity. The same also holds for LH bands. This allows us to define the chirality operator^{10,12} which reads,

$$\hat{\chi}_z = \begin{pmatrix} \hat{i}_z & 0 & 0 & 0 \\ 0 & \hat{i}_z & 0 & 0 \\ 0 & 0 & -\hat{i}_z & 0 \\ 0 & 0 & 0 & -\hat{i}_z \end{pmatrix}, \quad (3)$$

where \hat{i}_z is the inversion operator with respect to the z variable. The $\hat{\chi}_z$ operator has 2 eigenvalues, which we denote by \uparrow , and \downarrow . In the case of $\chi_z = \uparrow$, the Luttinger spinors have even parity with respect to z for the first two components of the spinor and odd parity with respect to z for the last two components of the spinor. In the case of $\chi_z = \downarrow$, the parity pattern is reversed between the first two and last two components of the spinor. Furthermore, square QDs also have parity symmetry in the $x-y$ plane, and we may define another parity operator $\hat{\chi}_{xy}$ analogous to the $\hat{\chi}_z$ by replacing \hat{i}_z with $\hat{i}_x \hat{i}_y$ on the diagonal terms in Eq.(3) where \hat{i}_x and \hat{i}_y are inversion operators along the x and the y direction respectively. Arguments for the $\hat{\chi}_z$ operator also apply to the $\hat{\chi}_{xy}$ operator. The only difference is that the \hat{R} operator in Eq.(2) involves $(k_-)^2$ term which prevents further separation of x and y variables. Again, $\hat{\chi}_{xy}$ has 2 eigenvalues denoted by $\chi_{xy} = +1$ and $\chi_{xy} = -1$. For $\chi_{xy} = +1$, the first two components of the spinor must have the same parity with respect to x and y , and the last two components of the spinor must have opposite parity with respect to x and y . For $\chi_{xy} = -1$, the Luttinger spinors again have the parity pattern switched between the first two and last two components.

The 4-band valence hole spinors in a square QD have well defined structures. The Bloch function part of the Luttinger spinors is determined by the lattice symmetries; while the envelope function part of Luttinger spinors is obtained from Eq.(1). In our analysis, we

expand the envelope function of the Luttinger spinors in eigenstates of the 3D infinite potential well of the size of our computational box. As mentioned, the chirality and the $x - y$ parity symmetries allow us to label Luttinger spinors by χ_z , χ_{xy} , and N , which index the N^{th} eigenstate of subspace χ_z and χ_{xy} . For instance, the N^{th} state of the subspace $\chi_z = \uparrow$ and $\chi_{xy} = +1$ reads

$$|\uparrow, +1, N\rangle = \sum_{\substack{n+m=2p-1 \\ n'+m'=2p}} \begin{pmatrix} C_{nm1}^{\uparrow,+1,N,3/2} \xi_n(x) \xi_m(y) \cos\left(\frac{\pi z}{W_z}\right) \left| \frac{3}{2} \right\rangle \\ C_{nm1}^{\uparrow,+1,N,-1/2} \xi_n(x) \xi_m(y) \cos\left(\frac{\pi z}{W_z}\right) \left| -\frac{1}{2} \right\rangle \\ C_{n'm'2}^{\uparrow,+1,N,1/2} \xi_{n'}(x) \xi_{m'}(y) \sin\left(\frac{2\pi z}{W_z}\right) \left| \frac{1}{2} \right\rangle \\ C_{n'm'2}^{\uparrow,+1,N,-3/2} \xi_{n'}(x) \xi_{m'}(y) \sin\left(\frac{2\pi z}{W_z}\right) \left| -\frac{3}{2} \right\rangle \end{pmatrix}, \quad (4)$$

where $p = 1, 2, 3, \dots$ are positive integers. $C_{nml}^{\chi_z, \chi_{xy}, N, J_z}$ represents the coefficient for the envelope function of a specific component $|J_z\rangle$ of Luttinger spinors. In our study, we assume that the confinement along the z direction is strong, so we only need to consider the first 2 eigenfunctions of the 1D infinite potential well in this direction. $\xi_{s_r}(r) = \sqrt{\frac{2}{W_r}} \cos\left(\frac{s_r \pi r}{W_r}\right)$ if s_r is odd and $\sqrt{\frac{2}{W_r}} \sin\left(\frac{s_r \pi r}{W_r}\right)$ if s_r is even. W_r is the computation box length along the r direction. $|J_z = \pm\frac{3}{2}, \pm\frac{1}{2}\rangle$ represents the Bloch functions¹⁹ of zincblende structure with the total angular momentum projection J_z . The Luttinger spinors in other subspaces have distinguishable parity patterns derived from Eq.(4) by switching either the parity pattern with respect to the $x - y$ variable or the z variable between first two and last two components of the spinor.

From here onwards, the Luttinger spinor is written with the components corresponding to the Bloch functions in the order $J_z = 3/2, -1/2, +1/2, -3/2$ as done in Eq.(4), and we will no longer explicitly write out the Bloch functions $|J_z\rangle$ as we have done above.

III. HOLE STATES IN SINGLE QUANTUM DOT

In this analysis, we take the entire Luttinger spinor as a representation of valence hole state confined in the quantum dots as opposed to adopting the HH single band approximation^{7,8}. Due to the time reversal symmetry, we have a doubly degenerate ground state with distinct chirality at zero field. We encode the qubit with the chirality, χ_z , of the ground state Luttinger spinors. We show that static magnetic fields applied along the z and the x direction indeed act as $\hat{\sigma}_x$ and $\hat{\sigma}_z$ operators respectively in the qubit subspace. This

result assures all the basic ingredients needed to perform arbitrary single qubit rotations.

A. Hole under B_z field

By diagonalizing the LK Hamiltonian for a square QD, we find that the 2 ground states are characterized by quantum numbers $(\chi_z = \uparrow, \chi_{xy} = -1)$ and $(\chi_z = \downarrow, \chi_{xy} = +1)$ respectively. Let us denote the state with $|\chi_z = \uparrow\rangle$ by $|1\rangle$, and the other state with $|\chi_z = \downarrow\rangle$ by $|0\rangle$. We give an approximate form of the envelope wave functions

$$|1\rangle = \begin{pmatrix} a\xi_1(x)\xi_1(y)\xi_1(z) \\ b\xi_2(x)\xi_2(y)\xi_1(z) \\ [c_1\xi_1(x)\xi_2(y) + c_2\xi_2(x)\xi_1(y)]\xi_2(z) \\ [d_1\xi_1(x)\xi_2(y) + d_2\xi_2(x)\xi_1(y)]\xi_2(z) \end{pmatrix}, \quad (5)$$

where $\xi_1(r) = \sqrt{\frac{2}{W_r}} \cos\left(\frac{\pi r}{W_r}\right)$ and $\xi_2(r) = \sqrt{\frac{2}{W_r}} \sin\left(\frac{2\pi r}{W_r}\right)$. $|0\rangle$ is obtained by applying the time reversal operator to $|1\rangle$. According to Kramer's degeneracy theorem, $|0\rangle$ will have the same set of envelope functions in Eq.(5) but complex conjugated and in a reversed order in the spinor. Due to the strong confinement along the z direction, the ground states of the system will contain a dominant contribution from the HH states. Therefore, the states $|0\rangle$ and $|1\rangle$ correspond to either a $+3/2$ HH or $-3/2$ HH occupying the $(1, 1, 1)$ orbital of a 3D infinite potential box.

To analyze the system in the presence of external fields \mathbf{B} , we use the gauge $\mathbf{A} = (-B_z y/2, B_z x/2, B_x y - B_y x)$. First, we consider the system under an external field B_z . Fig 2a shows the energy spectrum of a single square dot charged with one valence hole as a function of B_z . We see that the qubit subspace, the 2 lowest energy levels, are well isolated from the rest of the energy spectrum across a wide range of applied field. Due to the weak coupling between the qubit subspace and other excited states, we may treat the effects of B_z fields by the first order Löwdin perturbation theory²⁰, which is simply a projection of the full LK Hamiltonian into the qubit subspace. The entire LK Hamiltonian is decomposed into 2 parts: unperturbed Hamiltonian at the zero field and additional perturbing Hamiltonian due to the field. The additional Hamiltonian with external field B_z leads to $\hat{P}_1^{+(-)}$ operators

of the form

$$\begin{aligned}\hat{P}_1^+ &= \frac{\hbar^2}{2m_0}(\gamma_1 + \gamma_2) [(\omega_z)^2(x^2 + y^2) + \omega_z(xk_y - yk_x)], \\ \hat{P}_1^- &= \frac{\hbar^2}{2m_0}(\gamma_1 - \gamma_2) [(\omega_z)^2(x^2 + y^2) + \omega_z(xk_y - yk_x)],\end{aligned}\tag{6}$$

where $\omega_z = \frac{eB_z}{\hbar}$. Whether the applied field can break the chirality symmetry $\hat{\chi}_z$ and the x-y parity symmetry $\hat{\chi}_{xy}$ depends on the commutation relations between $\hat{P}_1^{+(-)}$ operators and inversion operators \hat{i}_z and $\hat{i}_x\hat{i}_y$. Since $\hat{P}_1^{+(-)}$ commute with \hat{i}_z , the Hamiltonian can not mix the 2 spinors of different chiralities. Indeed, when we project the Hamiltonian we find the off-diagonal matrix elements $\langle 1|\hat{H}_{LK}|0\rangle = 0$, and the diagonal matrix elements $\langle 1|\hat{H}_{LK}|1\rangle$ and $\langle 0|\hat{H}_{LK}|0\rangle$ differ only by the Zeeman energy. The diagonal matrix elements read,

$$\begin{aligned}\langle 1|\hat{H}_{LK}|1\rangle &= \kappa\Omega(|a|^2 - |d_1|^2 - |d_2|^2)(3/2) + \\ &\quad \kappa\Omega(-|b|^2 + |c_1|^2 + |c_2|^2)(1/2), \\ \langle 0|\hat{H}_{LK}|0\rangle &= -\langle 1|\hat{H}_{LK}|1\rangle,\end{aligned}\tag{7}$$

where the coefficients a, b, c, d are defined in Eq.(5). As the ground state of flat QDs has dominant contributions from HH components, typically $|a|^2 \approx 0.9$ is much greater than the magnitude of other coefficients. In HH single band approximation, one simply sets $|a| = 1$ and other coefficients to be 0.

B. Hole under B_x field

Next, we consider the system subject to a constant B_x field. Fig 2b shows the energy spectrum of a single square QD charged with one valence hole as a function of B_x . The two qubit states are again well isolated from the rest of the energy spectrum across a wide range of B_x . Hence, we repeat the same procedure to derive an effective Hamiltonian for the qubit. The vector potential is $\mathbf{A} = (0, 0, B_x y)$ and the $\hat{P}_1^{+(-)}$ operators for the additional LK Hamiltonian with B_x field read

$$\begin{aligned}\hat{P}_1^+ &= \frac{\hbar^2}{2m_0}(\gamma_1 - 2\gamma_2) [(\omega_x)^2 y^2 - 2\omega_x y k_z], \\ \hat{P}_1^- &= \frac{\hbar^2}{2m_0}(\gamma_1 + 2\gamma_2) [(\omega_x)^2 y^2 - 2\omega_x y k_z],\end{aligned}\tag{8}$$

where $\omega_x = \frac{eB_x}{c\hbar}$. We find that the diagonal matrix elements $\langle 1|\hat{H}_{LK}|1\rangle = \langle 0|\hat{H}_{LK}|0\rangle$, and the off-diagonal matrix elements are given by

$$\begin{aligned} \langle 1|\hat{H}_{LK}|0\rangle &= \langle g^{-3/2}|\hat{P}_1^+|g^{3/2}\rangle + \langle g^{3/2}|\hat{P}_1^+|g^{-3/2}\rangle + \\ &\quad \langle g^{-1/2}|\hat{P}_1^-|g^{1/2}\rangle + \langle g^{1/2}|\hat{P}_1^-|g^{-1/2}\rangle - \\ &\quad \langle g^{-1/2}|\hat{S}^*|g^{3/2}\rangle + \langle g^{3/2}|\hat{S}^*|g^{-1/2}\rangle - \\ &\quad \langle g^{-3/2}|\hat{S}|g^{1/2}\rangle + \langle g^{1/2}|\hat{S}|g^{-3/2}\rangle, \\ &\approx \Omega_x(\gamma_1 - 2\gamma_2)\frac{W_y}{W_z}Im(d_1^*a). \end{aligned} \quad (9)$$

where $\Omega_x = \hbar eB_x/mc$. $|g^i\rangle$ stands for the envelope function of the i hole states in Eq.(5), for instance, $\langle \mathbf{r}|g^{3/2}\rangle = a\xi_1(x)\xi_1(y)\xi_1(z)$. The matrix elements $\langle g^{-3/2}|\hat{P}_1^+|g^{3/2}\rangle$ do not suggest coupling of $+3/2$ HH and $-3/2$ HH. Rather, it actually represents the coupling of a chirality up ($\chi_z = \uparrow$) $+3/2$ HH with a chirality down ($\chi_z = \downarrow$) $+3/2$ HH. Due to time reversal symmetry, the chirality down $+3/2$ HH must have the same envelope function as the chirality up $-3/2$ HH. Similar argument applies to all other matrix elements in Eq.(9). We further remark that the off-diagonal matrix element contains pairs of complex conjugates; thus, the matrix element is real-valued.

The mixing of the qubit states is due to the simultaneous breaking of the parity symmetry in the $x - y$ plane and the inversion symmetry along the z direction; for instance, we refer to the term yk_z in both \hat{P}_1^+ and \hat{P}_1^- operators in Eq.(8) as responsible for the breaking of symmetries. The fact that we may couple the qubit states by static fields is in contradiction to analysis done in the HH single band approximation⁸. In HH single band approximation, the single qubit operation cannot be done by electron spin resonance (ESR) techniques because the magnetic field cannot couple two HH states (in the leading dipole approximation). More sophisticated techniques such as electric dipole spin resonance (EDSR) are needed. However, in our proposal, we define qubit states with the entire Luttinger spinor, which is an admixture of all HHs and LHs, and the mixing of the two qubit states is due to the coupling between the two Luttinger spinors as manifested in Eq.(9).

The $\hat{\sigma}_z$ operator for our proposed Luttinger spinor based qubit is essentially driven by the Zeeman energy; whereas the $\hat{\sigma}_x$ operator is based on the mixing of valence hole components by vector potential \mathbf{A} and SO coupling. Due to the different mechanisms of how the 2 qubit states are operated on by B_z and B_x field, the effective g factor (for a simple spin in an external field) seems to have much stronger transverse component²¹, $g_{\perp} \gg g_{//}$. Hence it

takes more time to perform a spin flip process with the Luttinger spinor based qubit. We will characterize the single qubit operating time with the $\hbar/\Delta E_{gap}$, where ΔE_{gap} is the energy difference between ground and first excited state under B_x field. From Fig 2b, we see the characteristic time is around 1.5 ns when $B_x = 1T$. However, modulating the strain of the host material can relax the QD confinement along the z direction, induce a stronger planar component of the g factors and improve the single qubit operating time.

Finally, we remark that the Luttinger spinor based qubits are susceptible to the same channels of decoherence that are already discussed for valence hole confined in QDs in Refs. 9,22–24. However, electric field fluctuation in the background of the host material will not affect the Luttinger spinor based qubits. As the electric field induced dipole transitions, $\langle \psi_j | e\mathbf{E}(t) \cdot \mathbf{r} | \psi_i \rangle$, conserve the time reversal symmetry, the two qubit states, which are Kramers doublets, will not be mixed.

IV. HOLE STATES IN COUPLED QUANTUM DOTS

We now turn to the analysis of double qubit operations with the Luttinger spinors based qubits. Our proposal for double qubit operations with the valence holes-based qubits relies on the following assumptions. First, we consider 2 valence holes localized in two different QDs in the weak tunneling limit and only the on-site Coulomb interaction is taken into account. Second, we consider that each QD only contains the two relevant qubit states. Under these assumptions, the hole-hole interacting Hamiltonian in second quantization reads¹²

$$\begin{aligned}
H_{2h} = & \sum_{j,p} \epsilon_{jp} c_{jp}^\dagger c_{jp} + \sum_j t \left(c_{jp'}^\dagger c_{jp} + c_{jp}^\dagger c_{jp'} \right) \\
& + \frac{1}{2} \sum_{\substack{j_{1p}, j_{2p} \\ j_{3p}, j_{4p} \\ p}} U_{j_{1p}j_{2p}j_{3p}j_{4p}} c_{j_{1p}}^\dagger c_{j_{2p}}^\dagger c_{j_{3p}} c_{j_{4p}}, \tag{10}
\end{aligned}$$

where p are indices for QD number 1 and 2, $p \neq p'$, ϵ_{jp} is the energy of valence hole state $|j\rangle$ on the p -th dot, t is the tunneling parameter between QDs, and $U_{j_1j_2j_3j_4}$ is the on-site Coulomb interaction, with the matrix elements given in the appendix. This Hamiltonian can be greatly simplified because the Coulomb interaction conserves the chirality of 2 holes in the following manner: (a) if $\chi_{z_1} = \chi_{z_2}$ and $\chi_{z_3} = \chi_{z_4}$, $U_{j_1j_2j_3j_4} = U_c$, (b) if $\chi_{z_1} \neq \chi_{z_2}$ and $\chi_{z_3} \neq \chi_{z_4}$, $U_{j_1j_2j_3j_4} = U_x$, (c) if just one of the valence holes switches chirality, $U = 0$.

Taking also into account that we only consider 2 states of distinct chirality on each QD, the on-site Coulomb interactions term in Eq.(10) reduces to¹²

$$U = \frac{1}{2}(U_c + U_x) \hat{n}_j \hat{n}_{j'}, \quad (11)$$

where $\hat{n}_{j(j')}$ is the number operator, and j, j' represents the 2 chirality states on a QD. Different from electron spins, the on-site Coulomb interaction between valence holes is composed of a direct Coulomb term U_c and an exchange term U_x which enhance the overall interaction. However, apart from this difference, once we have parameterized the tunneling parameter t and U , we have the Hubbard Hamiltonian. In the strong Coulomb regime, the interaction between 2 localized particles in the Hubbard model can be reduced to two spins with the Heisenberg exchange constants J proportional to t^2/U .

An interesting phenomenon¹¹ associated with valence holes is the possibility of engineering t to be either positive, zero or negative in a stack of vertically coupled cylindrical QDs by simply tuning the inter-dot distance. As the exchange coupling between 2 qubits is directly proportional to t^2 , this implies qubit-qubit interactions can be turned on and off as needed. We would like to investigate whether the similar phenomenon will happen with square QDs stacked either in a vertical or lateral structure.

To estimate the magnitude of t , we rely on a tight-binding picture in which a valence hole tunnels between the two dots and the hybridization of local orbitals gives a symmetric state, $1/\sqrt{2}(|1\rangle + |2\rangle)$ with energy $E_0 - t$ and an antisymmetric state, $1/\sqrt{2}(|1\rangle - |2\rangle)$ with energy $E_0 + t$. Thus, the energy gap between first excited state and ground state is $2t$. So we compute the energy spectrum of a single valence hole in a double QDs by exact diagonalizing Eq.(1), then we extract the value of t from the calculated energy gap.

A. Hole states in vertically coupled quantum dots

The potential $V(\mathbf{r})$ of VCQDs is modeled with an infinite potential well along the x and the y direction and double well potential profile along the z direction. In the barrier region between the dots, we set a constant finite potential of 320 meV corresponding to the band offset between InGaAs and GaAs, same as reported in Ref. 10, so we may draw a comparison between square-like and disk-like dots.

As shown in Fig 3a, the lowest energy levels of different chirality subspaces cross at a

certain inter-dot distance. The insets of Fig 3a present the most dominant HH wavefunction profile along the z direction of the ground state before and after the crossing point. The wavefunction plots show the reversal of symmetry for the ground state of the system. Similar phenomenon occurs in both square and disk dots. These results confirm that the effects of HH and LH mixing is insensitive to the confining potential in the $x - y$ plane. These results also imply that we can shut down any undesirable hole - hole interaction between holes localized in different dots if the inter-dot distance is chosen at the point where the crossing occurs in Fig 3a.

B. Hole states in laterally coupled quantum dots

The potential of LCQDs is modeled similar to that of VCQDs except that the double well potential profile lies along the y direction. Our result, Fig 3b, shows no crossing of lowest energy states from distinct chirality subspaces. We understand that the confinement strength along the z direction plays a crucial role in determining how much HH and LH bands mixing a system will experience, because QDs are quasi-two dimensional devices with a much smaller dimension along the z direction. In the case of VCQDs, the coupled dots relax significantly the confinement strength of the hole states along the z direction and bring the LH and HH energies closer. However, a LCQDs structure relaxes confinement strength in the $x - y$ plane which does not facilitate the mixing of HH and LH states. Hence no reversal of the ground state as a function of the distance is observed.

V. CONCLUSION

In summary, we consider the Luttinger spinor description of confined valence hole states in QDs. We identify the two qubit levels with two chiralities of the lowest energy Kramers doublet and suggest that B_z and B_x fields act analogously to the $\hat{\chi}_z$ and $\hat{\chi}_x$ operators. For arrays of hole qubits we study tunneling of holes in vertical and lateral architecture as dominant mechanism for the qubit exchange interaction. We show that tunneling can be arrested for vertical pairs of quantum dots but not for lateral architecture. The capability to switch the sign of the effective tunneling t in VCQDs is demonstrated. This suggests the possibility of turning off the exchange interaction. With such exchange interaction being

very small one can envisage tuning this interaction with additional metallic gates.

Acknowledgments

The authors thank NSERC, NRC-CNRS-CRP, QuantumWorks and CIFAR for support.

Appendix: On-site Coulomb matrix elements

The on-site Coulomb matrix elements among valence hole states $|j_i\rangle = |\chi_{z_i}\chi_{xy_i}, N_i\rangle$ can be evaluated as follows

$$U_{j_1 j_2 j_3 j_4} = \frac{e^2}{8\pi^3 \epsilon_0} \sum_{J_{z_1}, J_{z_2}} \sum_{\substack{n_i, m_i, l_i \\ i=1,2,3,4}} C_{n_1, m_1, l_1}^{*\chi_{z_1}, \chi_{xy_1}, N_1, J_{z_1}} C_{n_2, m_2, l_2}^{*\chi_{z_2}, \chi_{xy_2}, N_2, J_{z_2}} C_{n_3, m_3, l_3}^{\chi_{z_3}, \chi_{xy_3}, N_3, J_{z_2}} C_{n_4, m_4, l_4}^{\chi_{z_4}, \chi_{xy_4}, N_4, J_{z_1}} \iiint d^3q \frac{1}{q^2} G_{n_1 n_2 n_3 n_4}(x, x', q_x) G_{m_1 m_2 m_3 m_4}(y, y', q_y) G_{l_1 l_2 l_3 l_4}(z, z', q_z), \quad (\text{A.1})$$

where ϵ_0 is the static dielectric constants of InGaAs. We define

$$G_{s_1 s_2 s_3 s_4}(r, r', q_r) = \iint dr dr' \xi_{s_1}(r) \xi_{s_4}(r) \xi_{s_2}(r') \xi_{s_3}(r') e^{iq_r |r-r'|}. \quad (\text{A.2})$$

-
- ¹ J. A. Brum and P. Hawrylak, *Superlattices Microstruct.* **22**, 431 (1997).
² D. Loss and D. P. DiVincenzo, *Phys. Rev. A* **57**, 120 (1998).
³ G. Burkard, D. Loss, and D. P. DiVincenzo, *Phys. Rev. B* **59**, 2070 (1999).
⁴ R. Hanson, L. P. Kouwenhoven, J. R. Petta, S. Tarucha, and L. Vandersypen, *Rev. Mod. Phys.* **79**, 1217 (2007).
⁵ A. Sachrajda, P. Hawrylak, and M. Ciorga, *Nano-spintronics with lateral quantum dots* ("Electronic Transport in Quantum Dots", ed. by J. P. Bird, Kluwer Academic Publishers, Boston, 2003).
⁶ M. Korkusinski and P. Hawrylak, *Coded qubits based on electron spins* (in book "Semiconductor quantum bits", ed. by O. Benson and F. Henneberger, World Scientific, 2008).
⁷ B. D. Gerardot, D. Brunner, P. A. Dalgarno, P. Öhberg, M. K. S. Seidi, K. Karrai, N. G. Stoltz, P. M. Petroff, and R. J. Warburton, *Nature* **451**, 441 (2007).

- ⁸ D. V. Bulaev and D. Loss, Phys. Rev. Lett. **98**, 097202 (2007).
- ⁹ D. V. Bulaev and D. Loss, Phys. Rev. Lett **95**, 076805 (2005).
- ¹⁰ J. I. Climente, M. Korkusinski, G. Goldoni, and P. Hawrylak, Phys. Rev. B **78**, 115323 (2008).
- ¹¹ M. F. Doty, J. I. Climente, M. Korkusinski, M. Scheibner, A. S. Bracker, P. Hawrylak, and D. Gammon, Phys. Rev. Lett **102**, 047401 (2009).
- ¹² L. G. C. Rego, P. Hawrylak, and J. A. Brum, A. Wojs, Phys. Rev. B **55**, 15694 (1997).
- ¹³ F. V. Kyrychenko and J. Kossut, Phys. Rev. B **70**, 205317 (2004).
- ¹⁴ F. B. Pedersen and Y.-C. Chang, Phys. Rev. B **53**, 1507 (1996).
- ¹⁵ T. Darnhofer, U. Rössler, and D. A. Broido, Phys. Rev. B **52**, R14376 (1995).
- ¹⁶ D. A. Broido, A. Cros, and U. Rössler, Phys. Rev. B **45**, 11395 (1992).
- ¹⁷ P. C. Sercel and K. J. Vahala, Phys. Rev. B **42**, 3690 (1990); K. J. Vahala and P. C. Sercel, Phys. Rev. Lett **65**, 239 (1990).
- ¹⁸ M. Reimer, W. McKinnon, J. Lapointe, D. Dalacu, P. J. Poole, G. C. Aers, D. Kim, M. Korkusinski, P. Hawrylak, and R. L. Williams, Physica E **40**, 1790 (2007).
- ¹⁹ J. M. Luttinger and W. Kohn, Phys. Rev. **97**, 869 (1955).
- ²⁰ P.-O. Löwdin, J. Chem. Phys. **19**, 1396 (1951).
- ²¹ H. W. van Kesteren, E. C. Cosman, W. A. J. A. van der Poel, and C. T. Foxon, Phys. Rev. B **41**, 5283 (1990).
- ²² L. M. Woods, T. L. Reinecke, and R. Kotlyar, Phys. Rev. B. **69**, 125330 (2004).
- ²³ S. Laurent, B. Eble, O. Krebs, A. Lemaitre, B. Urbaszek, X. Marie, T. Amand, and P. Voisin, Phys. Rev. Lett. **94**, 147401 (2005).
- ²⁴ Y. A. Serebrennikov, Phys. Lett. A **372**, 3307 (2008).

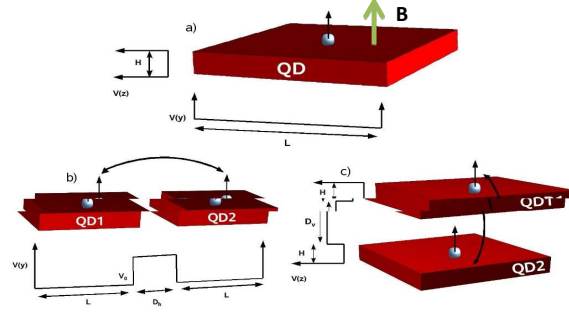


FIG. 1: Schematics of (a) square vertically coupled quantum dots (VCQDs) of side lengths $L=20\text{nm}$ and height $H=2\text{nm}$ separated by a potential barrier V_0 of width D_v along the vertical direction. (b) Square laterally coupled quantum dots (LCQDs) of same side lengths L , height H separated by a potential barrier V_0 of width D_h along the horizontal direction.

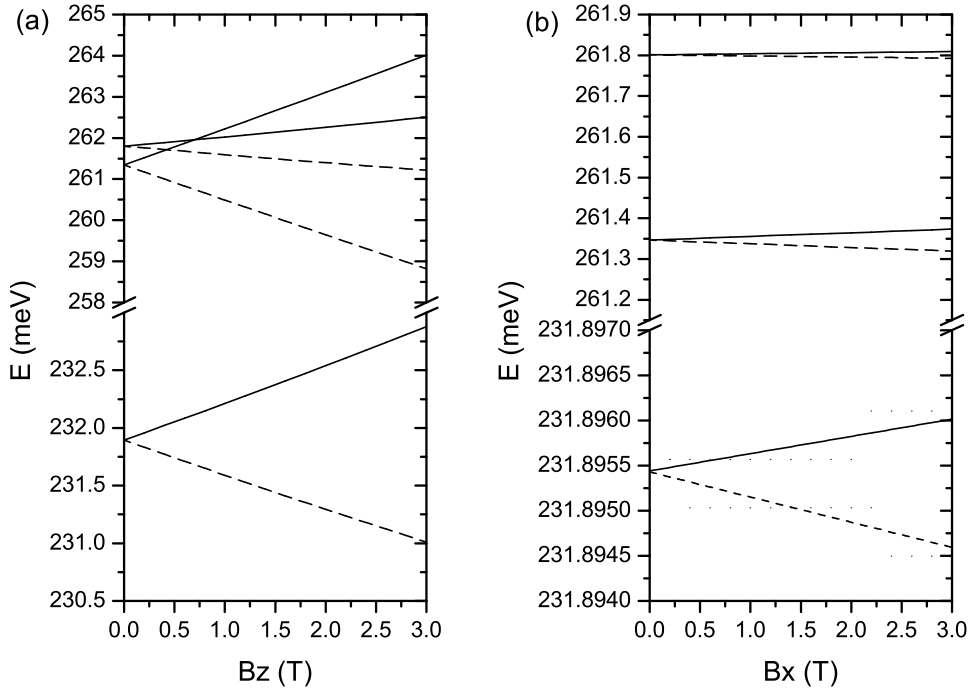


FIG. 2: Energy levels of the 6 lowest lying hole states as a function of (a) magnetic field B_z (applied in the z direction) and (b) magnetic field B_x (applied in the x direction).

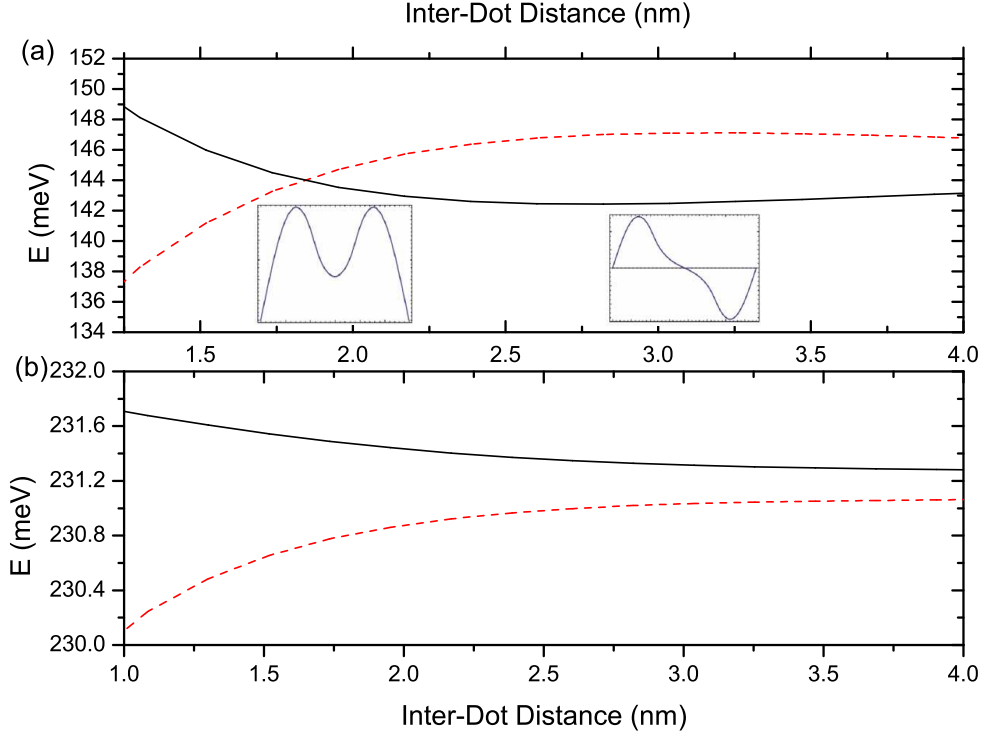


FIG. 3: Energy levels of the two lowest hole states as a function of the inter-dot distance in: (a) VCQDs (vertically coupled quantum dots) and (b) LCQDs (laterally coupled quantum dots). The critical distance at which the tunneling element is zero occurs around 1.8 nm in (a). The solid curve represents $\chi_z = \uparrow$ state and the dashed curve represents the $\chi_z = \downarrow$ state. Inset: The dominant heavy hole component of the ground state before and after the crossing.